Phase diagrams of Zwanzig models: The effect of polydispersity

Yuri Martínez-Ratón* and José A. Cuesta†

Grupo Interdisciplinar de Sistemas Complejos (GISC),
Departamento de Matemáticas, Universidad Carlos III de Madrid,
Avda. de la Universidad 30, E–28911, Leganés, Madrid, Spain.
(Dated: February 2, 2008)

The first goal of this article is to study the validity of the Zwanzig model for liquid crystals to predict transitions to inhomogeneous phases (like smectic and columnar) and the way polydispersity affects these transitions. The second goal is to analyze the extension of the Zwanzig model to a binary mixture of rods and plates. The mixture is symmetric in that all particles have equal volume and length-to-breadth ratio, κ. The phase diagram containing the homogeneous phases as well as the spinodals of the transitions to inhomogeneous phases is determined for the cases $\kappa = 5$ and 15 in order to compare with previous results obtained in the Onsager approximation. We then study the effect of polydispersity on these phase diagrams, emphasizing the enhancement of the stability of the biaxial nematic phase it induces.

PACS numbers: 64.70.Md,64.75.+g,61.20.Gy

I. INTRODUCTION

Although the Zwanzig model was introduced long ago as a very simplified model to study the isotropic-nematic transition in liquid crystals [1], the determination of its phase diagram, including all inhomogeneous bulk phases, has never been carried out so far. With the help of the scaled-particle theory (equivalent to a $y3$ expansion), developed for a variety of hard particle fluids [2] including the hard parallelepipeds with restricted orientations which define the Zwanzig model [3], the phase behavior of the homogeneous bulk phases has been investigated. Also the the isotropic-nematic interface has been accessible to calculations through a smoothed-density approximation [3], which consists in evaluating the bulk free energy at some smoothed density, following the same recipe of Tarazona for hard spheres [4].

The usual second virial approximation (exact for freely rotating models but only approximate for restricted orientation models) has recently been applied to the Zwanzig model in order to elucidate the bulk phase behavior of a polydisperse mixture of hard rods [5]. With an inhomogeneous version of this approximation different interfaces of a monodisperse hard rod fluid [6], as well as its polydisperse counterpart [7], have been studied.

Unlike for hard objects with free orientations—like spherocylinders, which have been extensively simulated [9], there is only one simulation of the Zwanzig model in a square lattice [10], for parallelepipeds with dimensions $5 \times 1 \times D$ (with $D =1$, rods, or 5, plates) [10]. The main reason for this lack of simulation data is that any Monte Carlo movement which includes reorientation of parallelepipeds to any of the three directions has a very low acceptance ratio due to the huge overlap between particles as the length-to-breadth ratio and the density increase.

The second virial approximation of the free energy of the Zwanzig model has also been employed to investigate the phase diagram of symmetric mixtures of rods and plates [11]. Stimulated by theoretical calculations made in the early 70's [12] which show that a binary mixture of rods and plates can stabilize a biaxial nematic phase (in which the symmetry axes of particles of different types point along mutually perpendicular directions), van Roij and Mulder studied the relative stability of this phase against a nematic-nematic phase separation [11]. The authors calculated the phase diagram for different length-to-breadth ratios $\kappa \equiv L/D$. They showed that for $\kappa > 8.8$ the biaxial phase is stable in a relative small window above a multicritical point. How the topology of these phase diagrams is modified when a scaled-particle approximation (which includes higher order virial coefficients) is used instead of the second virial is one of the open questions which we will try to answer here. Another one is the influence of polydispersity in the phase behavior of the mono and bidisperse Zwanzig model. This is most relevant since with a recently derived a fundamental measure functional (FMF) for hard parallelepipeds [13] (equivalent to the scaled-particle theory for homogeneous phases), we have shown that polydispersity may enhance the thermodynamic stability of a biaxial nematic phase [14].

There are recent experiments on true mixtures of hard rods and plates which show a very rich phase behavior, including triple coexistence between an isotropic and two nematics—each rich in one of the species—as well as inhomogeneous phases, like a columnar phase [15]. This phase behavior has been quantitatively accounted for using the Parson approximation of the free energy functional of binary mixture of rods and plates in the Onsager limit [16]. Nevertheless, the long searched biaxial phase has not been found in these experiments. An unavoidable ingredient of experiments is polydispersity. In Ref. [14]

*Electronic address: yuri@math.uc3m.es
†Electronic address: cuesta@math.uc3m.es

we have shown that this otherwise undesirable element may cause the stabilization of the biaxial nematic phase. It is very important, though, that the system maintains rod-plate symmetry, in contrast with what happens in the existing experiments [15]. An open question in this work is the topology of the phase diagram at high packing fractions. Addressing this problem requires to study the possible phase transitions to inhomogeneous phases—like smectic, columnar and solid phases. The calculation of phase equilibria in polydisperse liquid crystals when one of the bulk phase is inhomogeneous is thus far a theoretical challenge. There is only one such work, which makes use of an approximate functional for length-polydisperse parallel hard cylinders to make two important predictions: the existence of a terminal polydispersity beyond which the smectic phase is no more stable, and the enhancement of the columnar phase stability [17]. These results have been confirmed in simulations of freely rotating hard spherocylinders in the Onsager limit [18].

The paper is organized as follows. In Sec. II A we describe both the model and the fundamental measure functional we will use to describe its free energy (A); the equations for phase equilibria between phases of a polydisperse system (B); and the formalism to determine spinodal instabilities in mono, bi or polydisperse systems (C). Section III describes the phase diagrams of the Zwanzig model without (A) and with polydispersity (B), as well as the bidisperse rod-plate model without (C) and with polydispersity (D). Finally we conclude in Sec. IV.

II. THEORY

A. Model

Let us consider a length-to-breadth polydisperse mixture of uniaxial oblate and prolate parallelepipeds, with their symmetry axes pointing along one of the three coordinate axes. Let us fix the volume of any particle to 1; thus if $\lambda = L/D$ is the length-to-breadth ratio (with L the length and D the breadth) of a parallelepiped, then

$$L = \lambda^{2/3}, \quad D = \lambda^{-1/3}. \tag{1}$$

Let us define $\rho^\nu(\lambda)$ to be the density distribution function of the species parallel to the ν $(= x, y, z)$ axis, and let the total number density to be

$$\rho = \int_0^\infty d\lambda\, \rho(\lambda), \qquad \rho(\lambda) = \sum_\nu \rho^\nu(\lambda). \tag{2}$$

The (temperature reduced) free energy density of a multicomponent mixture is given by $\beta F V^{-1} \equiv \Phi = \Phi_{\rm id} + \Phi_{\rm exc}$, where $\Phi_{\rm id}$ is the ideal part, whose exact form is

$$\Phi_{\rm id} = \sum_{\nu,i} \rho_i^\nu \left(\ln \rho_i^\nu - 1\right), \tag{3}$$

i labeling different components, and the excess part, $\Phi_{\rm exc}$, can be approximated by the FMF for hard parallelepipeds [13], namely

$$\Phi_{\rm exc} = -n_0 \ln(1 - n_3) + \frac{\sum_\nu n_1^\nu n_2^\nu}{1 - n_3} + \frac{\prod_\nu n_2^\nu}{(1 - n_3)^2}, \tag{4}$$

where the weighted densities $\{n_\alpha\}$ have the form

$$n_0 = \sum_{\nu,i} \rho_i^\nu \equiv \rho, \quad n_1^\nu = \sum_i \left[\rho D_i + \rho_i^\nu (L_i - D_i)\right], \tag{5}$$

$$n_3 = \sum_{\nu,i} \rho_i^\nu L_i D_i^2, \quad n_2^\nu = \sum_i \left[\rho L_i - \rho_i^\nu (L_i - D_i)\right] D_i. \tag{6}$$

Specializing the above expressions for our polydisperse mixture and using Eq. (1) we obtain

$$\Phi_{\rm id} = \sum_\nu \int_0^\infty d\lambda \rho^\nu(\lambda) \left[\ln \rho^\nu(\lambda) - 1\right], \tag{7}$$

$$\Phi_{\rm exc} = -\rho \ln(1 - \rho) + \frac{\sum_\nu \xi_-^\nu \xi_+^\nu}{1 - \rho} + \frac{\prod_\nu \xi_+^\nu}{(1 - \rho)^2}, \tag{8}$$

$$\xi_\pm^\nu = \int_0^\infty \lambda^{\pm 1/3} \left[\left(\lambda^{\mp 1} - 1\right) \rho^\nu(\lambda) + \rho(\lambda)\right]. \tag{9}$$

The pressure can be obtained from its definition

$$\beta\Pi = \sum_\nu \int_0^\infty d\lambda \left[\rho^\nu(\lambda)\Phi^\nu(\lambda)\right] - \Phi, \tag{10}$$

$$\Phi^\nu(\lambda) \equiv \frac{\delta\Phi}{\delta\rho^\nu(\lambda)}, \tag{11}$$

which in this particular case yields

$$\beta\Pi = \frac{\rho}{1 - \rho} + \frac{\sum_\nu \xi_-^\nu \xi_+^\nu}{(1 - \rho)^2} + \frac{2 \prod_\nu \xi_+^\nu}{(1 - \rho)^3}. \tag{12}$$

B. Phase equilibria between homogeneous phases

To obtain the phase equilibria we follow the general procedure already reported elsewhere [5, 21]. Suppose that among the n coexisting phases there are n_I isotropic, n_N nematic and n_B biaxial phases ($n = n_I + n_N + n_B$). The global density distribution (the parent distribution) is fixed to be

$$P(\lambda) = P_0 h(\lambda), \quad \int d\lambda h(\lambda) = 1, \tag{13}$$

so total mass conservation of each species is expressed by the lever rule

$$P(\lambda) = \sum_{a=1}^n \gamma_a \rho_a(\lambda), \tag{14}$$

with $\rho_a(\lambda)$ the total density distribution of phase a and γ_a the fraction of the total volume it occupies (there is the obvious constraint $\sum_a \gamma_a = 1$). Minimizing the free

energy density Φ with respect to the fraction of particles with length-to-breadth ratio λ oriented along the ν axis, i.e. $p_a^\nu(\lambda) \equiv \rho_a^\nu(\lambda)/\rho_a(\lambda)$, and using Eq. (14), the equality of the chemical potentials of each species in different phases

$$\beta\mu_a(\lambda) = \sum_\nu \rho_a^\nu(\lambda)\Phi_a^\nu(\lambda), \qquad (15)$$

leads to the following expressions for the coexisting densities

$$\rho_a^\nu(\lambda) = P_0 h(\lambda)\frac{e^{-\Phi_a^\nu(\lambda)}}{\sum_b \gamma_b \sum_\tau e^{-\Phi_b^\tau(\lambda)}} \qquad (16)$$

The parent distribution we are going to use throughout the paper is characterized by

$$h(\lambda) = \lambda^{-1}\left[\zeta f(\lambda/\kappa) + (1-\zeta)f(\lambda\kappa)\right], \qquad (17)$$
$$f(z) = K_0(\alpha)^{-1}\exp\left[-(\alpha/2)\left(z^2 + z^{-2}\right)\right], \qquad (18)$$

where $K_\nu(\alpha)$ $(\alpha > 0)$ is the νth-order modified Bessel function, and $\kappa > 1$. This choice is motivated by its rod-plate symmetry for $\zeta = 1/2$. The best way to appreciate this symmetry is changing the variable to $\ln\lambda$: $\tilde{h}(\ln\lambda) = \lambda h(\lambda)$ has two identical humps (wider the smaller α) centered at $\ln\kappa$ (rods of "typical" aspect ratio κ) and $-\ln\kappa$ (plates of typical aspect ratio κ^{-1}). The parameter $0 \leq \zeta \leq 1$ allows one to tune the overall composition of the mixture, since the molar fraction of the rods is given by $x_r(\zeta) = \int_1^\infty h(\lambda)d\lambda$ [and that of plates by $x_p(\zeta) = 1 - x_r(\zeta)$, of course]. Thus we can select polydisperse rods (plates) by setting $\zeta = 1$ $(\zeta = 0)$. The moments of this distribution are given by $\langle\lambda^m\rangle = K_{m/2}(\alpha)K_0(\alpha)^{-1}[\zeta\kappa^m + (1-\zeta)\kappa^{-m}]$, explicitly showing the symmetry of the mixture. A quantitative characterization of the polydispersity can be given if we determine the dispersion in L and D as obtained from $h(\lambda)$ for $\zeta = 0$ or 1. This yields

$$\Delta_{L,D} \equiv \sqrt{\frac{\langle\lambda^{2\nu/3}\rangle}{\langle\lambda^{\nu/3}\rangle^2} - 1} = \sqrt{\frac{K_{\nu/3}(\alpha)K_0(\alpha)}{K_{\nu/6}(\alpha)^2} - 1}, \quad (19)$$

where $\nu = 2$ for Δ_L and $\nu = 1$ for Δ_D.

The number of independent moments in the set $\{\rho, \xi_\pm^\nu\}$ which completely determine each coexisting phase is 3, 5 and 7 for the isotropic, nematic and biaxial phases respectively (which amounts to a total of $3n_I + 5n_N + 7n_B$ unknowns). They can be obtained through the definitions (2) and (9), together with the distribution functions (16). The remaining unknowns—the $n-1$ independent γ_α's—are calculated from the equality of pressures in every phase. This leaves the global dilution, P_0, as the control parameter. Alternatively, we can fix an external pressure, Π_0, and eliminate P_0 in terms of this new control parameter. As P_0 increases, the fractions of volume of each phase change; thus, for practical purposes, it is computationally simpler to use one of the γ_α's as control parameter and obtain P_0 as a function of it.

A particularly important case is the two phase coexistence between a phase (say β) which fills the whole volume (cloud phase) and an incipient new phase (say σ) which fills an infinitesimally amount of volume (shadow phase). In a cloud-shadow coexistence the parent $P(\lambda)$ coincides with the distribution function of the cloud phase. Then ρ and $\sum_\nu \xi_\pm^\nu$ are fixed for this phase, so the number of unknowns reduces by 3 (the number of constraints).

C. Spinodal instabilities with respect to inhomogeneous phases

In order to be as general as possible in developing the formalism let us consider the problem of finding the conditions for the stability of an arbitrary multicomponent system against spatial modulations of the densities ρ_i (i label the species). This way we can replace at the end $\sum_i \to \sum_\nu$ for the monodisperse Zwanzig model and $\sum_i \to \sum_\nu \int d\lambda$ for the polydisperse one, to obtain the respective spinodal instabilities. The reason for so proceeding is that, as we will show later, the spinodal equations can be expressed in two different ways, each of which suits one of the two cases.

The condition of equality of chemical potentials between two phases is equivalent to the minimization of the grand potential

$$\Omega = \int d\mathbf{r}\left\{k_B T\Phi(\{n_\alpha\}) - \sum_i \mu_i\rho_i(\mathbf{r})\right\}, \qquad (20)$$

at fixed chemical potentials of each species μ_i, with respect to the density profile of each species $\rho_i(\mathbf{r})$. We specify this grand potential for a general model whose free energy density Φ has an excess part depending on the densities only through certain weighted densities

$$n_\alpha(\mathbf{r}) = \sum_i \left[\rho_i * \omega_\alpha^i\right](\mathbf{r}), \qquad (21)$$

as it is the case of Rosenfeld's fundamental measure theory [19]. In the definition of n_α the symbol "$*$" stands for the convolution of two functions, i.e. $f * g(\mathbf{r}) \equiv \int d\mathbf{r}' f(\mathbf{r}')g(\mathbf{r} - \mathbf{r}')$.

We are concerned with the case when one of the coexisting phases is homogeneous and the other one is inhomogeneous, with its density profile consisting in a small perturbation around the homogeneous phase with density distribution ρ_i, i.e.

$$\rho_i(\mathbf{r}) = \rho_i\left[1 + \epsilon_i(\mathbf{r})\right], \qquad \epsilon_i(\mathbf{r}) \ll 1. \qquad (22)$$

The result of minimizing (20) with respect to $\rho_i(\mathbf{r})$ can be cast as

$$\rho_i(\mathbf{r}) = \rho_i \exp\left\{-\sum_\alpha \left[\Delta\phi_\alpha * \omega_\alpha^i\right](\mathbf{r})\right\}, \qquad (23)$$

where $\Delta\phi_\alpha(\mathbf{r}) = \phi_\alpha(\mathbf{r}) - \phi_\alpha$ and $\phi_\alpha = \partial\phi/\partial n_\alpha$. We are implicitly using magnitudes without spatial variable arguments to denote homogeneous phase quantities. Expanding $\Delta\phi_\alpha(\mathbf{r})$ to first order in $\epsilon_i(\mathbf{r})$ yields

$$\Delta\phi_\alpha(\mathbf{r}) = \sum_\beta \phi_{\alpha\beta} \sum_j \rho_j \left[\epsilon_j * \omega_\beta^j\right](\mathbf{r}) + \cdots, \qquad (24)$$

where $\phi_{\alpha\beta} = \partial^2\Phi/(\partial n_\alpha \partial n_\beta)$. Inserting (24) in (23) and expanding the exponential again to first order in $\epsilon_i(\mathbf{r})$ we arrive at the integral equation

$$\epsilon_i(\mathbf{r}) = -\sum_{\alpha,\beta} \phi_{\alpha\beta} \sum_j \rho_j \left[\epsilon_j * \omega_\alpha^i * \omega_\beta^j\right](\mathbf{r}), \qquad (25)$$

which is handier to write in Fourier space

$$\varepsilon_i(\mathbf{q}) + \sum_{\alpha,\beta} \phi_{\alpha\beta}\Omega_\alpha^i(\mathbf{q}) \sum_j \rho_j\varepsilon_j(\mathbf{q})\Omega_\beta^j(\mathbf{q}) = 0, \qquad (26)$$

where ε and Ω are respectively the Fourier transforms of ϵ and ω [with the usual definition $f(\mathbf{q}) = \int d\mathbf{r}\, e^{i\mathbf{q}\mathbf{r}} f(\mathbf{r})$].

Equation (26) gets clearer if written in matrix form. Defining the functions

$$m_{ij}(\mathbf{q}) \equiv \sum_{\alpha,\beta} \phi_{\alpha\beta}\Omega_\alpha^i(\mathbf{q})\Omega_\beta^j(\mathbf{q}), \qquad (27)$$

the matrices $\hat{\mathrm{M}}(\mathbf{q}) \equiv \left(m_{ij}(\mathbf{q})\right)$ and $\hat{\mathrm{P}} \equiv \left(\rho_j\delta_{ij}\right)$, and the vector $\boldsymbol{\varepsilon}(\mathbf{q}) \equiv \left(\varepsilon_i(\mathbf{q})\right)$, Eq. (26) becomes

$$\left(\mathrm{I} + \hat{\mathrm{M}}(\mathbf{q})\cdot\hat{\mathrm{P}}\right)\boldsymbol{\varepsilon}(\mathbf{q}) = 0, \qquad (28)$$

where I is the identity matrix. This linear system has nontrivial solutions if and only if

$$D(\rho,\mathbf{q}) \equiv \det\left[\mathrm{I} + \hat{\mathrm{M}}(\mathbf{q})\cdot\hat{\mathrm{P}}\right] = 0. \qquad (29)$$

This equation is suitable for the cases in which there is a small number of components, like the monodisperse Zwanzig model with only three components: $\nu = x, y, z$.

Alternatively we can multiply (26) by $\rho_i\Omega_\gamma^i(\mathbf{q})$, sum over i and define the functions

$$u_\gamma(\mathbf{q}) \equiv \sum_i \rho_i\varepsilon_i(\mathbf{q})\Omega_\gamma^i(\mathbf{q}); \qquad (30)$$

then Eq. (26) becomes

$$u_\gamma(\mathbf{q}) + \sum_{\alpha,\beta} \phi_{\alpha\beta}n_{\alpha\gamma}(\mathbf{q})u_\beta(\mathbf{q}) = 0, \qquad (31)$$

where we have introduced new functions

$$n_{\alpha\gamma}(\mathbf{q}) = \sum_i \rho_i\Omega_\alpha^i(\mathbf{q})\Omega_\gamma^i(\mathbf{q}). \qquad (32)$$

Equation (31) can also be written in matrix form, but now the indices run over the set of weights, not the components. Hence, defining the matrices $\hat{\Phi} \equiv \left(\phi_{\alpha\beta}\right)$

and $\hat{\mathrm{N}}(\mathbf{q}) \equiv \left(n_{\alpha\gamma}(\mathbf{q})\right)$, and the vector $\mathbf{u}(\mathbf{q}) \equiv \left(u_\alpha(\mathbf{q})\right)$, Eq. (31) becomes

$$\left[\mathrm{I} + \hat{\mathrm{N}}\cdot\hat{\Phi}\right]\mathbf{u} = \mathbf{0}. \qquad (33)$$

Again this system has nontrivial solutions if and only if

$$D(\rho,\mathbf{q}) \equiv \det\left[\mathrm{I} + \hat{\mathrm{N}}\cdot\hat{\Phi}\right] = 0. \qquad (34)$$

This alternative characterization of the spinodal is suitable for polydisperse systems (actually, it is a generalization of the formalism developed in Ref. [20] for homogeneous phases). The reason is that it replaces integral operators by finite matrices, in which the number of components is limited by the number of weights of the theory. For instance, for the polydisperse Zwanzig model with a free energy functional given by the FMF derived in Ref. [13], functions $n_{\alpha\beta}$ take the form

$$n_{\alpha\beta}(\mathbf{q}) = \sum_\nu \int d\lambda\, \rho^\nu(\lambda)\Omega_\alpha^\nu(\mathbf{q},\lambda)\Omega_\beta^\nu(\mathbf{q},\lambda), \qquad (35)$$

where $\alpha,\beta = 0, (1x,1y,1z), (2x,2y,2z), 3$ and

$$\Omega_0^\nu(\mathbf{q},\lambda) = \prod_k w_0(q_k\Lambda_{\nu k}), \qquad (36)$$

$$\Omega_3^\nu(\mathbf{q},\lambda) = \prod_k \Lambda_{\nu k}w_3(q_k\Lambda_{\nu k}), \qquad (37)$$

$$\Omega_{1,k}^\nu(\mathbf{q},\lambda) = \Lambda_{\nu k}w_1(q_k\Lambda_{\nu k})\Omega_0^\nu(\mathbf{q},\lambda), \qquad (38)$$

$$\Omega_{2,k}^\nu(\mathbf{q},\lambda) = \left[\Lambda_{\nu k}w_1(q_k\Lambda_{\nu k})\right]^{-1}\Omega_3^\nu(\mathbf{q},\lambda) \qquad (39)$$

$(k = x, y, z)$. Here q_k are the components of the vector $\mathbf{q}$, and

$$\Lambda_{\nu k} = \lambda^{-1/3} + (\lambda^{2/3} - \lambda^{-1/3})\delta_{\nu k}, \qquad (40)$$

$$w_0(x) = \cos(x/2), \qquad (41)$$

$$w_3(x) = 2\sin(x/2)/x, \qquad (42)$$

$$w_1(x) = w_3(x)/w_0(x). \qquad (43)$$

As there are 8 different weights, $D(\rho,\mathbf{q})$ is in this case the determinant of an 8×8 matrix.

Either way we express the equation, (29) or (34), the spinodal instability condition of a homogeneous phase with density distributions $\rho^\nu(\lambda)$ (or simply ρ^ν in the monodisperse case) with respect to the transition to an inhomogeneous phase occurs at the values of the total density ρ and wave vector $\mathbf{q}$ for which the function $D(\rho,\mathbf{q})$ first vanishes. More precisely, this function has an oscillatory behavior as a function of $\mathbf{q}$, and is positive as long as the homogeneous phase is stable, so the spinodal corresponds to the smallest density ρ for which the absolute minimum of D with respect to $\mathbf{q}$ equals zero. This amounts to finding, for a given ρ, the solutions to

$$\boldsymbol{\nabla}D(\rho,\mathbf{q}) = 0. \qquad (44)$$

When we later consider the rod-plate mixture we will have to locate the nematic-biaxial phase transition. As

it is a continuous transition it can also be found as a solution to Eq. (34) with $\mathbf{q} = 0$ (both phases are homogeneous), using

$$\rho^\nu(\lambda) = P_0 h(\lambda) \frac{e^{-\Phi^\nu(\lambda)}}{\sum_\tau e^{-\Phi^\tau(\lambda)}} \qquad (45)$$

as the distribution functions of the nematic phases.

III. RESULTS

A. Monodisperse Zwanzig model

As a first step towards the calculation of the whole phase diagram of the monodisperse (pure rods or pure plates) Zwanzig model using the FMF of Ref. [13] we will determine the isotropic-nematic (I–$N^\pm$) coexistence curves as well as the spinodals for the nematic-smectic ($N^\pm$–$S^\pm$), nematic-columnar ($N^\pm$–$C^\pm$) and isotropic-plastic (orientationally disordered) solid (I–PS) transitions, as a function of the length-to-breadth ratio κ. The $+$ and $-$ superscripts label prolate (rods) and oblate (plates) parallelepipeds respectively. If the transitions are first order, the location of the coexistence curves will differ from that of the corresponding spinodals. However, as the main concern of this paper is the effect of polydispersity, we defer the calculations of coexistence with and between inhomogeneous phases to a forthcoming publication.

We have obtained the spinodals for this model by solving Eqs. (29) and (44) using the monodisperse version of (45). If we choose the nematic director parallel to the z axis, then the $N^\pm$–$S^\pm$ spinodals can be calculated setting $\mathbf{q} = (0, 0, q)$, whereas the $N^\pm$–$C^\pm$ ones follow from taking $\mathbf{q} = (q, 0, 0)$ or $\mathbf{q} = (0, q, 0)$ (both are equivalent due to the nematic symmetry). For the I–PS spinodal all three previous vectors give the same result.

Figure 1 shows the results of these calculations. We observe in this figure that there is I–$N^\pm$ transition only for $\kappa < 0.210$ and $\kappa > 5.02$. At those two limiting values of κ the N^+ phase is destabilized by a S^+ at a packing fraction $\rho = 0.280$, and the N^- by a C^- at a packing fraction $\rho = 0.261$ (remember the particle volume has been set to 1). Also, the N^+–S^+ spinodal is always below the N^+–C^+, and the N^-–C^- spinodal is always below the N^-–S^- one. This is what intuition tells us but, as we will see later, it is a peculiarity of the monodisperse system. Despite this, all these spinodal curves converge asymptotically to the same packing fraction, $\rho = 0.314$, as $\kappa \to \infty$ or $\kappa \to 0$. This is precisely the packing fraction at which the continuous freezing transition occurs in a system of parallel hard cubes ($\kappa = 1$) [22]. The reason for this is that upon increasing κ the number of rods with orientation perpendicular to the director becomes vanishing small, and then the system is, after rescaling the z direction, almost equivalent to a system of parallel cubes. The same holds for plates upon decreasing κ. What this
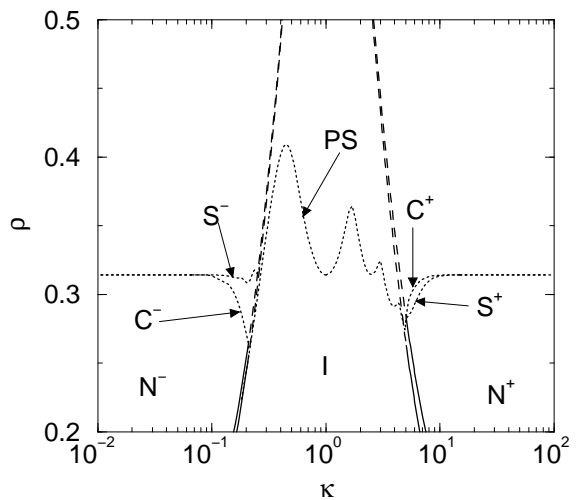

FIG. 1: Phase diagram (packing fraction, ρ, vs. length-to-breadth ratio, κ) of the monodisperse Zwanzig model. Solid and dashed lines represent the isotropic (I)-nematic ($N^\pm$) coexistence curves. The dashed lines correspond to the values for which the homogeneous phases are unstable with respect to the inhomogeneous ones. Dotted lines represent the spinodals of the different homogeneous phases: each one is labeled with the corresponding phase: smectic ($S^\pm$), columnar ($C^\pm$) or plastic solid (PS).

means is that most likely the N^+–S^+ and N^-–C^- transitions will be metastable with respect to freezing in a large portion of the phase diagram. For $0.182 < \kappa < 4.93$ we have found an I–PS spinodal instability. The peculiarity of this curve is that it exhibits strong oscillations as the aspect ratio changes. These oscillations reflect the packing efficiency of randomly oriented parallelepipeds as a function of their size (the better the packing the lower the curve).

The available simulation results for freely rotating hard spherocylinders show that the I–S^+ and N^+–S^+ transitions begin at $\kappa = 4.1$ and 4.5 respectively [9] (notice that for hard spherocylinders the length-to-breadth ratio is $\kappa = \frac{L+D}{D}$). On the other hand, simulations of hard cut spheres show that for $\kappa = 0.2$ there is an I–C^- transition (the isotropic phase might instead be a peculiar 'cubatic' phase) and for $\kappa = 0.1$ a N^-–C^- one [8]. We can see that despite the different particle geometry and the restricted orientations of the Zwanzig model, the agreement with the threshold κ's at which spatial instabilities destabilize the homogeneous phases is rather good. Also the qualitative picture is similar: elongated rods form smectics, while flat disks form columnars, and more symmetric particles form solids instead of smectics or columnar. Thus, this simple model seems to capture the essence of the entropy driven phase transitions between phases with different symmetries and their relation to particle anisotropy.

The only existing simulation of the Zwanzig model has been performed on a lattice model of parallelepipeds

with length-to-breadth ratios 15 : 3 ($\kappa = 5$) and 3 : 15 ($\kappa = 0.2$) [10]. For these κ's the authors find I–C$^-$ for the discs and and I–DS$^+$ for the rods, where DS$^+$ stands for a novel phase called 'discotic smectic' by the authors (in this phase the axes of the particles point perpendicular to the normal of the smectic layers while there is no orientational order within the layer). The packing fractions they obtain for the transitions are higher than those of the corresponding spinodals of Fig 1, but they should decrease upon decreasing the lattice spacing, as the results for the freezing of parallel hard cubes on a lattice (occurring at $\rho = 0.568$ for edge-length 2 lattice spacings, at $\rho = 0.402$, for edge-length 6 lattice spacings, and at $\rho = 0.314$ for the continuum) illustrate [24]. All this is again in agreement with the phase diagram of Fig. 1.

B. Polydisperse Zwanzig model: Unimodal distribution

Let us study now the effect polydispersity has on the phase behavior of the Zwanzig model discussed above. We have introduced polydispersity through the unimodal parent probability density resulting when setting $\zeta = 1$ (rod-like parallelepipeds) or $\zeta = 0$ (plate-like parallelepipeds) in function (17). Before reporting the results we have obtained, a few words on polydisperse phase diagram plots are on purpose.

Generally speaking, plotting polydisperse phase diagrams would require an infinite dimensional space, for as we vary the fraction of total volume occupied by the coexisting phases they change their composition. A phase diagram like that of Fig. 1 plots densities vs. aspect ratios, thus carrying no information whatsoever about compositions. So we must restrict ourselves to a given composition, and this is the parent one, since all pure phases have this composition. This means that only cloud lines can be plotted, delimiting regions where we can only know that the system is decomposed into two or more coexisting phases. The result resembles the coexisting lines of monodisperse phase diagram, but the meaning is completely different. Although we could connect cloud points in the two lines delimiting the coexistence region, they are definitely no coexisting states.

Similar considerations hold for spinodal lines. We can represent the spinodal of a system in a pure phase having the parent distribution as composition, but if the system reaches a cloud point an incipient shadow phase with a totally different composition—hence a totally different spinodal line—coexists with it. If the density of this shadow phase is above its own spinodal line, the phase transition will not be stable.

Having all this in mind we have solved the coexistence equations of the isotropic and nematic phases and determined the spinodal lines of inhomogeneous instabilities for a system with the parent distribution (17). The results for the choice $\alpha = 1$ (corresponding to polydispersity parameters $\Delta_L = 0.288$ and $\Delta_D = 0.143$) are shown
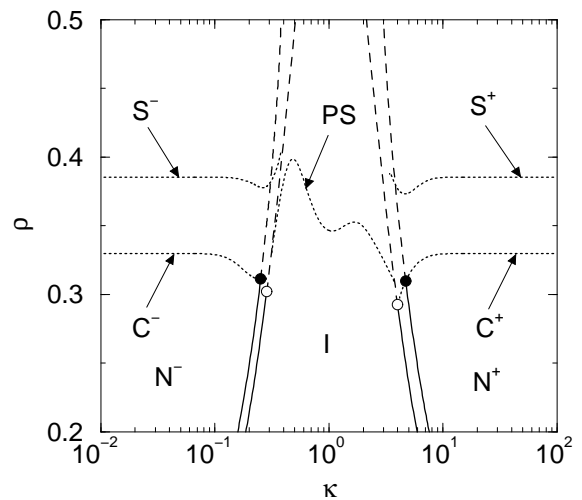

FIG. 2: Phase diagram for polydisperse Zwanzig model. The distribution of aspect ratios is unimodal with the maximum at κ. Polydispersity is $\Delta_L = 0.288$ in length and $\Delta_D = 0.143$ in breadth. The lines have the same meanings as in Fig. 1. Full circles mark the points above which the nematic cloud phase is unstable against columnar ordering; empty circles mark the points above which the isotropic cloud phase coexists with a nematic shadow phase unstable against columnar modulations (the spinodal line of this nematic shadow, computed with the corresponding aspect ratio distribution, is not plotted in the figure).

in Fig. 2.

Apart from the usual broadening of the isotropic-nematic transition already observed for this model in Ref. 5, we find a clear enhancement of the stability of the homogeneous phases i.e. the spinodal instabilities occur at higher densities. This effect is more pronounced for the N$^\pm$–S$^\pm$ or N$^\pm$–C$^\pm$ transitions. Another remarkable feature of Fig. 2 is that the columnar phases are by far more stable than the smectic ones for any aspect ratio.

This general behavior is in agreement with the results obtained from both density functional theory for length-polydisperse parallel hard cylinders [17] and computer simulations for length-polydisperse freely rotating hard spherocylinders in the Onsager limit [18]. Although in Ref. [17] some strong approximations were made, such as the decoupling of the density profile as $\rho(\mathbf{r}, L) = g(L)\rho(\mathbf{r})$, and the effect of fractionation between the nematic and columnar phases was ignored, the results agree qualitatively with the simulations: both show a terminal polydispersity beyond which the smectic phase is no more stable, being replaced by a columnar phase (which tolerates a higher degree of polydispersity). The nematic-columnar transition is first order. While fractionation is indeed negligible in the nematic-smectic transition, the smectic-columnar transition clearly segregates long rods into the columnar phase.

It is interesting to notice that in the limits $\kappa \to \infty$

or 0 none of the spinodal lines tend to the density of the freezing of parallel hard cubes ($\kappa = 1$). The reason is that no trivial scaling can be applied to a polydisperse system of perfectly aligned parallelepipeds to transform it into a system of parallel hard cubes. On the other hand the S^+ and S^- spinodals tend to the same limiting density when $\kappa \to 0, \infty$, and so do the C^+ and C^- spinodals. The second virial term of the free energy is dominant for large (small) κ's; this and the rod-plate symmetry of the chosen parent distributions explains this behavior.

C. Binary mixture of Zwanzig rods and plates

We have calculated the phase diagram (coexistence of homogeneous phases as well as their spinodal instabilities to inhomogeneous phases) for the binary mixture of rods and plates with $\kappa = 5$ and 15. The results for $\kappa = 5$ are shown in Fig. 3. Apart from the usual I–N$^\pm$ transitions and N$^-$–N$^+$ phase separations which coalesce in a multicritical point we see that the nematic phases increase their stability with respect to the inhomogeneous ones as the relative composition of the fluid tends to the equimolar mixture. Another important feature is that the biaxial nematic is not stable.

All these characteristics are also present in the phase diagram obtained using a second virial approximation [11], but there are important differences as well. The most prominent one is that the whole phase diagram is shifted down in density, with all transitions and spinodals appearing below $\rho = 0.4$ (those obtained with a second virial approximation occur above that value [11]). This result should not surprise if one takes into account that in a $y3$ expansion the excess free energy is written in terms of the variable $y = \rho/(1 - \rho)$, which grows faster than ρ. Another striking difference with respect to the second virial approach is the rod-plate asymmetry of the phase diagram, a consequence of the inclusion of higher virial coefficients—which do not share the symmetry of the second one.

We pass now to describe the loss of stability of the nematics with respect to inhomogeneous phases. The intersection between the N$^+$ line of the I–N$^+$ coexistence and the N$^+$–C$^+$ spinodal in the rod-rich part of the phase diagram (marked in the figure with a full circle; the open circle corresponds to its coexisting isotropic phase) is consistent with the existence of a first order phase transition between the I phase and an inhomogeneous (presumably columnar) phase. (Recall that simulations on the lattice find a first order I-DS$^+$ transition for parallelepipeds with $\kappa = 5$ [10]). Nevertheless a definitive answer about the relative stability between these inhomogeneous phases—including also the solid—can only be given after carrying out coexistence calculations.

Increasing the fraction of plates (which in the C$^+$ phase have their principal axes oriented perpendicular to the director) seems to favor the smectic alignment of rods. This results in the intersection of the N$^+$–C$^+$ and the
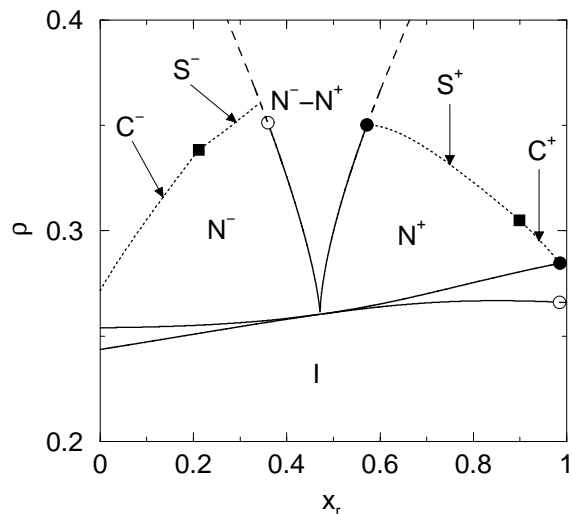

FIG. 3: Phase diagram of a binary mixture of rods and plates with $\kappa = 5$; x_r is the fraction of rods and ρ coincides with the packing fraction. Spinodal and coexistence curves are represented by dotted and solid lines, respectively. Dashed lines are coexistence curves in the unstable region. The crossings between the coexistence curves and the spinodals are represented with full circles, and with empty circles their coexisting phases. Full squares mark the crossover between columnar and smectic phases along the spinodals.

N$^+$–S$^+$ spinodals (marked with a full square on the right of Fig. 3). In the second virial approach the N$^+$–S$^+$ spinodal is always below the N$^+$–C$^+$ one. At the plate-rich part of the phase diagram the nematic exhibits a spinodal to the C$^-$ phase, as usual in discotic fluids [8]. Increasing the fraction of rods beyond a threshold value (indicated with a full square on the left part of the phase diagram) makes the smectic more stable than the columnar, which agrees qualitatively with the results from the second virial approach [11].

The phase diagram for $\kappa = 15$ appears in Fig. 4. Its main difference with the previous one is the presence of a thermodynamically stable biaxial nematic phase in an inverted triangular right above the multicritical point. The window is limited to the left and to the right by continuous phase transitions to uniaxial nematic phases, and to the top by a B–N$^+$ coexistence which becomes a N$^-$–N$^+$ phase separation as density increases. As discussed in Ref. [11], the driving mechanism which determines the preference of this system for phase separation instead of biaxial ordering is the larger exclude volume between unlike particles compared to that of like particles (the rod-plate excluded volume divided by the rod-rod one scales as $\kappa^{2/3}$ for large κ). When the gain in free volume compensates the loss in mixing entropy (and this strongly depends on concentration and composition) phase separation occurs.

The slight asymmetry of the phase diagram is again due to the presence of higher virial terms in the free energy. The second virial approximation predicts a small
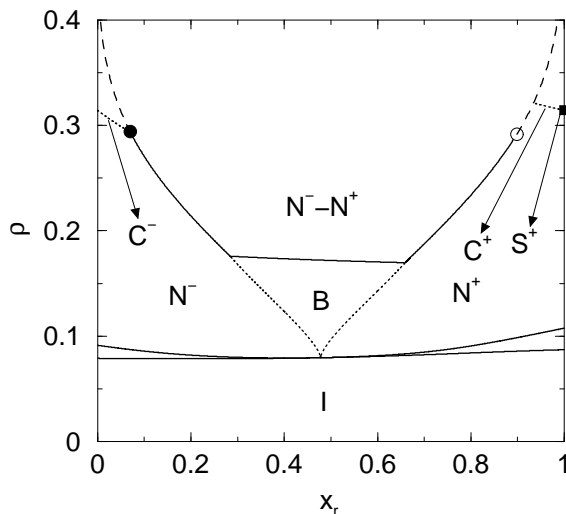
FIG. 4: Phase diagram of binary mixture of rods and plates with $\kappa = 15$. Lines and symbols have the same meanings as in Fig. 3. Notice that given the continuous nature of the B–N$^{\pm}$ transitions, the spinodals are the true transition lines.

region of triple coexistence between the N$^-$, N$^+$ and B phases right on top of the biaxial phase region. The absence of this triple coexistence region in Fig. 4 is due to the asymmetry of the phase diagram. Simulations of a mixture of prolate and oblate ellipsoids [25] show a similar asymmetric phase diagram, only tilted in the opposite direction (there is a B–N$^-$ demixing on top of the biaxial nematic, instead of the B–N$^+$ of the present model), probably due to the different particle geometry. Despite the asymmetry, we should admit that for $\kappa = 15$ there is good overall agreement between the second virial approach and ours.

We have not studied the changes an asymmetry in the mixture (a difference in the volume of rods and plates, for instance) would induce in the phase diagram. Intuitively, asymmetry acts against the stability of the biaxial phase, something that is confirmed by a recent work [26] which studies a binary rod-plate mixture of freely rotating oblate and prolate cylinders in the Onsager approximation. This work explicitly shows that the region of stability of the biaxial phase decreases with increasing the asymmetry of the mixture (although, according to this work, this phase can be found in highly asymmetry mixtures).

With respect to the inhomogeneous phases, Fig. 4 shows a remarkable behavior: although pure hard rods in the N$^+$ phase undergo a spinodal instability to a smectic one, by adding a tiny fraction of plates the instability takes place to a columnar phase. This phenomenon has already been observed in a different system, namely, in simulations of binary mixtures of parallel hard spherocylinders [27]. Although pure parallel hard spherocylinders exhibit a continuous nematic-smectic transition, a binary mixture of them with length-to-breadth ratios 2

and 2.9 show a first order nematic-columnar transition instead. This result was explained by the poorer packing of rods of different length in the smectic phase as compared to that of rods of the same length. Borrowing the argument, in our rod-plate model the plates can fit into the interlayer spacing with their axes parallel to the smectic director as long as there are few of them; but upon increasing their molar fraction some of them are forced to get into the smectic layers with their axes perpendicular to the smectic director, thereby destabilizing the smectic phase.

Finally, at the other extreme of phase diagram the N$^-$ phase losses its stability to a columnar phase of plates at densities lower than those of the N$^+$–C$^+$ spinodal.

D. Polydisperse Zwanzig model: Bimodal distribution

In this section we are going to study the effect of polydispersity on the phase behavior of the previous rod-plate mixture. In Ref. [14] we have shown how polydispersity can stabilize the biaxial phase even for mixtures with relative small aspect ratios—like $\kappa = 5$, for which Fig. 3 shows that the biaxial phase is absent.

Apart from the increase in mixing entropy that polydispersity carries, the other mechanism behind the enhancement of stability of the biaxial phase is the decrease of the ratio of the average exclude volumes of like and unlike particles. The excluded volume between two parallel rods with lengths L_i and breadth D_i ($i = 1, 2$) is

$$v_{rr} = (L_1 + L_2)(D_1 + D_2)^2, \qquad (46)$$

and the excluded volume between a rod with length L_1 and breadth D_1 and a plate with length L_2 and breadth D_2, with axes perpendicular to each other, is

$$v_{rp} = (L_1 + D_2)(L_2 + D_1)(D_1 + D_2). \qquad (47)$$

According to (1), if the volume of all particles is set to one, in terms of the length-to-breadth ratios λ_i, $L_i = \lambda_i^{2/3}$ and $D_i = \lambda_i^{-1/3}$. Taking a double average of v_{rr} over $\prod_i [h(\lambda_i)\Theta(\lambda_i - 1)]$ and of v_{rp} over $[\prod_i h(\lambda_i)]\Theta(\lambda_1 - 1)\Theta(1 - \lambda_2)$ [$h(\lambda)$ is the parent distribution (17)], and fixing $\zeta = 1/2$ (the equimolar composition) we arrive at

$$\frac{\langle\langle v_{rp}\rangle\rangle}{\langle\langle v_{rr}\rangle\rangle} = \frac{\frac{1}{2} + m_{-1}^2 + m_1^2 + 2(m_{-1}m_2 + m_1 m_{-2})}{\frac{1}{2} + 4m_{-1}m_1 + 2m_{-2}m_2}, \quad (48)$$

where $m_{\beta} \equiv \int_1^{\infty} d\lambda h(\lambda)\lambda^{\beta/3}$. It can be shown numerically that, for a given κ, the ratio (48) decreases with polydispersity (i.e. with decreasing α). Analytic expressions for this ratio can be obtained in the limit of high particle anisotropy ($\kappa \gg 1$) and high polydispersity ($\alpha \ll 1$) with the constraint $\alpha\kappa^2 \ll 1$ (in terms of the parameters Δ_{ν}, $\nu = L, D$, this constraint is equivalent to $1 \ll \Delta_{\nu} \ll \sqrt{\ln \kappa}$, implying that the fraction of cubic-like particles is vanishing small). Using the asymptotic
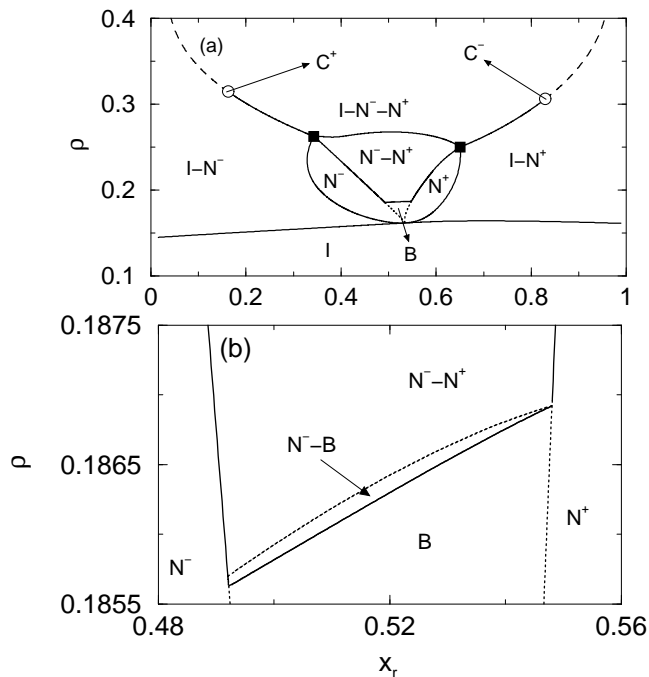
FIG. 5: Phase diagram of a polydisperse mixture of rods and plates with $\kappa = 5$ and length and breath polydispersities $\Delta_L = 0.610$ and $\Delta_D = 0.302$. Part (b) is a zoom of the region right above the biaxial phase.

α	Δ_L	Δ_D	κ^*
∞	0.000	0.000	6.9
2.00	0.216	0.107	6.6
1.00	0.288	0.143	6.3
0.50	0.374	0.185	5.9
0.25	0.470	0.233	5.1
0.10	0.610	0.302	4.0

TABLE I: Threshold values of the length-to-breadth ratio, κ^*, for the appearance of a biaxial nematic phase as a function of polydispersity, expressed in terms of the parameters α, Δ_L and Δ_D.

expressions

$$m_\beta \sim \frac{\kappa^{\beta/3}}{\alpha^{\beta/6}(-\ln\alpha)}, \qquad \Delta_\nu \sim (-\ln\alpha)^{1/2}, \qquad (49)$$

we obtain

$$\frac{\langle\langle v_{rp}\rangle\rangle}{\langle\langle v_{rr}\rangle\rangle} \sim \kappa^{2/3}e^{-c_\nu\Delta_\nu^2}, \quad \nu = L, D \qquad (50)$$

with c_ν a positive constant. This asymptotic relationship explicitly shows both the scaling of this ratio discussed for the pure rod-plate mixture [11] and the exponential attenuation of this scaling with polydispersity.

We have estimated the threshold value of κ (denoted κ^*) beyond which the biaxial phase begins to be thermodynamically stable, as a function of polydispersity. The

results are summarized in Table I. Without polydispersity this value is $\kappa^* = 6.9$, smaller than the second virial estimation [11] $\kappa^* = 8.8$. This is an indication that three (and higher) body correlations increase the stability of the biaxial phase. As we can see in Table I, κ^* decreases upon increasing polydispersity, an illustration of the enhancement of stability of the biaxial ordering induced by polydispersity.

In Fig. 5 we plot the phase diagram of this system for $\kappa = 5$ and $\alpha = 0.1$ (corresponding to $\Delta_L = 0.610$ and $\Delta_D = 0.302$). According to Table I for this parameter choice the biaxial phase is thermodynamically stable, and this is clearly shown in Fig. 5(a), where we can see a small window of biaxial nematic just above the multicritical point. Figure 5(b) is a zoom of the upper border of this window. There is a narrow region of N^-–B coexistence limited from above by a N^-–N^+ coexistence. The dividing line (the dotted line in the diagram) represents a continuous transition between the B and the N^+ phases which coexist with the N^-. This line has no analog in the binary rod-plate mixture. To obtain it one has to solve the equations for two phase coexistence at all values of γ in (16) (the volume occupied by one of the coexisting phases) and then find the one for which the B–N^+ transition occurs.

The high density part of the phase diagram of Fig. 5(a) was not determined in Ref. [14]. The most remarkable feature it shows is that pure phases are hardly stable: the diagram is dominated by coexistence regions. The reason is that polydispersity is so high that the mixture has, beside rods and plates, a significant amount of cubic-like particles. This favors entropic phase separation in the three different phases I, N^- and N^+.

In the upper part of Fig. 5(a) there is a region of triple coexistence I–N^-–N^+. The lines limiting this region were obtained by solving the coexistence equations for the case when one of the coexisting phases is a shadow phase (i.e. it occupies a vanishing fraction of the total volume). As an illustrative example, if we take $\gamma_I = 0$, $\gamma_{N^-} = \gamma$ and $\gamma_{N^-} = 1 - \gamma$ and solve the coexistence equations for the $N = 15$ unknowns (see the discussion about phase equilibria in polydisperse systems in Section II B) we obtain the curve joining the two points marked with full squares in Fig. 5(a). The other two curves limiting the triple coexistence region were calculated selecting $\gamma_{N^+} = 0$ (the left one) and $\gamma_{N^-} = 0$ (the right one).

We have checked that the nematics below the triple region are always stable with respect to spatial density modulations of any kind. In order to estimate the packing fraction at which these instabilities occur we solved Eqs. (34) and (44) using the density distributions $\rho^\nu(\lambda)$ of all the coexisting phases along the borders of the triple coexistence region. The left and right open circles correspond respectively to the packing fractions at which the coexisting N^+ and N^- (the shadow phase in both cases) lose their stability to the C^+ and C^- phases. Above these points the phase diagram will possibly include coexistences between four phases: I, N^-, N^+ and C^- or C^+)
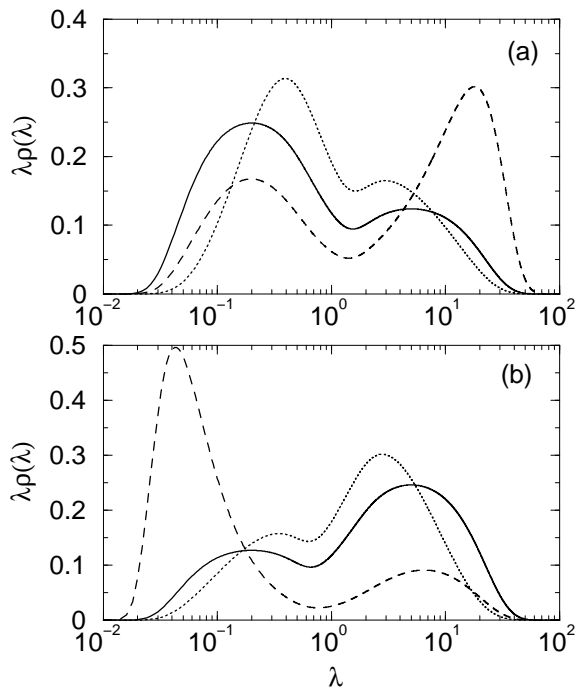
FIG. 6: Distribution functions at the N_{sh}^-–I–N^+ (a) and the N_{sh}^+–I-N^- (b) triple points of the phase diagram of Fig. 5 (marked with full squares). The subscript 'sh' denotes shadow phases. Solid lines represent the shadow phases, dotted lines the I phase and dashed lines the N^+ (a) and N^- (b) phases.

(the experiments of Ref. [15] find a similar scenario).

Figure 6 shows the density distribution functions of the phases coexisting at the points marked with full squares in Fig. 5(a). As already discussed, the curves illustrate the high fraction of cubic-like particles partly responsible for the strong demixing this system exhibits. The figure also illustrates the strong fractionation which takes place between the coexisting phases: the isotropic phase is rich in cubic-like particles, the N^- in plates and the N^+ in rods.

In contrast, the phase diagram of the polydisperse rod-plate mixture for $\kappa = 15$ does not change qualitatively compared to the binary mixture (cf. Figs. 7 and 4): the size and shape of the biaxial regions are similar and the general topology of the phase diagram is basically the same. The only important difference (minor in terms of the size of the portion of phase diagram it involves) appears just above the biaxial: one can observe both B–N^+ and B–N^- coexistence (the former occupying a larger region), as well as a triple coexistence zone separating them [see Fig. 7(c)]. As for $\kappa = 5$, the B–$N^\pm$ coexistences become N^+–N^- coexistence through a second order phase transition of the B phase to the $N^\pm$ [dotted lines in Fig. 7(b) and (c)].

The N^- and N^+ lose their stability to columnar phases at relative high packing fractions [see the dotted lines in the upper part of Fig. 7(a)]. In both cases it is the N^- phase which first becomes unstable with respect to C^- at
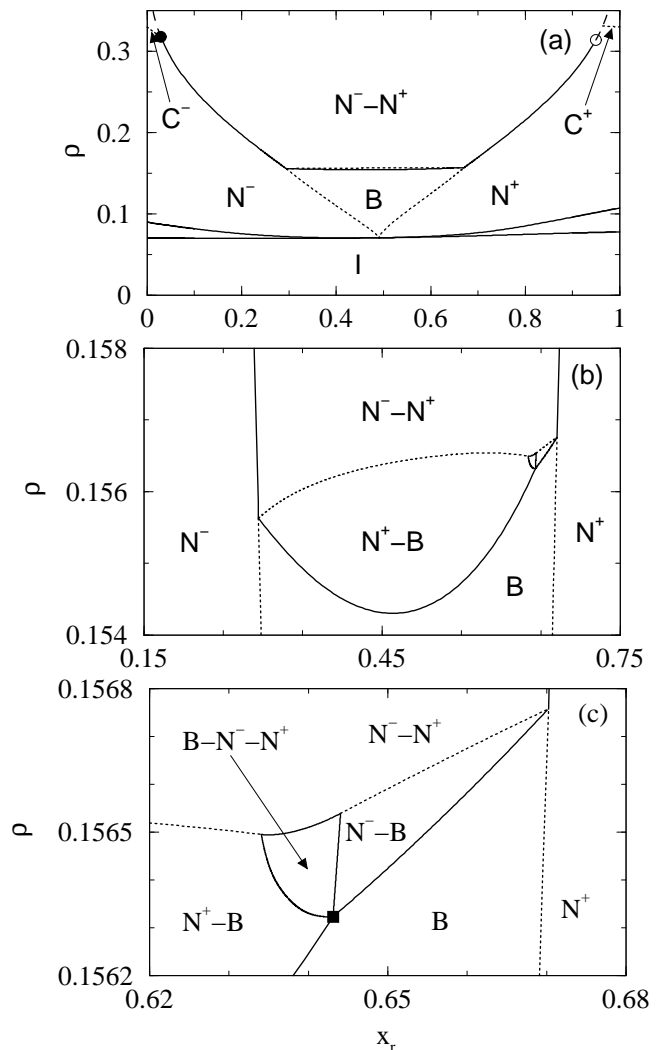

FIG. 7: Phase diagram and two details of a polydisperse rod-plate mixture with $\kappa = 15$ and length and breadth polydispersity $\Delta_L = 0.288$ and $\Delta_D = 0.143$, respectively.

the N^+–N^- coexistence (the N^- cloud on the left, marked with a full circle in Fig. 7(a), and the N^- shadow on the right, marked with an empty circle in this figure).

Figure 8 shows the density distribution functions corresponding to the point marked by a full square in Fig. 7(c). The distributions of the N^+ and B phases are very similar, except for the fact that the N^+ has a slightly higher proportion of rods (and correspondingly less of plates) than the B phase. It is clear from the figure that the proportion of cubic-like particles is negligible, so this mixture can be regarded as a true (polydisperse) rod-plate mixture.

IV. CONCLUSIONS

We have studied the effect of polydispersity on the phase diagrams of several variants of the Zwanzig model
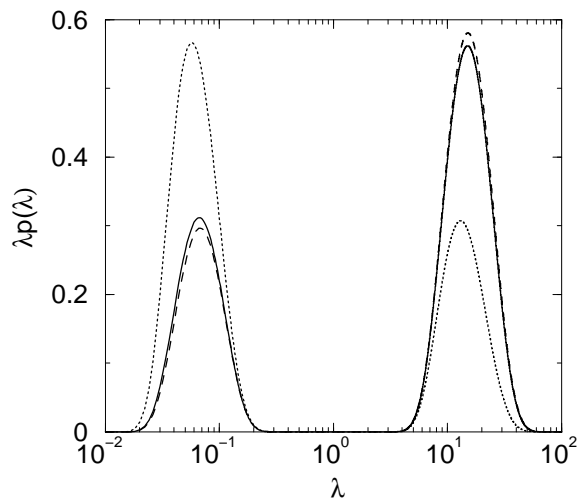
FIG. 8: Density distribution functions at the point marked with a full square in Fig. 7(c). The solid, dashed and dotted lines correspond to the cloud B, shadow N^+ and shadow N^- phases, respectively.

for liquid crystals. We have first determined the spinodal instabilities of the homogeneous phases to the smectic, columnar or plastic solid phases for one component fluids of rods or plates. There is a general qualitative agreement with phase diagrams of oblate and prolate particles obtained from Monte Carlo simulations [8, 9]. We have also shown that even a small degree of polydispersity has dramatic effects on the transitions to highly ordered phases (like the smectic or the columnar). In particular,

we have shown that upon increasing polydispersity the transition to the columnar phase of rods preempts the N^+–S^+ transition, in agreement with simulations [23].

Next we have obtained the phase diagrams of symmetric rod-plate binary mixtures with length-to-breadth ratios $\kappa = 5$ and 15. While for large κ's the differences between these phase diagrams and those calculated with a second virial approximation [11] are only quantitative, for small κ's both methods differ qualitatively. For instance, all the transitions occur at packing fractions well below those obtained with the second virial approach, and sometimes the relative stability between different inhomogeneous phases changes.

We have shown that the introduction of polydispersity in a rod-plate mixture in a very symmetric way enhances the stability of the biaxial phase even for as small an aspect ratio as $\kappa = 5$. For this case the amount of polydispersity needed to stabilize the biaxial phase is so high that the mixture becomes very unstable with respect to phase separation at practically any composition. There are large regions of three phase and possibly four phase coexistence (I–N^-–N^+ and I–N^-–N^+–$C^\pm$). These results agree with what is observed in experiments with rod-plate mixtures with a high degree of polydispersity [15].

[1] R. W. Zwanzig, J. Chem. Phys. **24**, 855 (1956); J. Chem. Phys. **39**, 1714 (1963).
[2] B. Barboy and W. M. Gelbart, J. Stat. Phys. **22**, 685 (1980).
[3] B. G. Moore and W. E. MacMullen, J. Phys. Chem. **96**, 3374 (1992); J. Chem. Phys. **97**, 9267 (1992).
[4] P. Tarazona, Mol. Phys. **52**, 81 (1984).
[5] N. Clarke, J. A. Cuesta, R. Sear, P. Sollich and A. Speranza, J. Chem. Phys. **113**, 5817 (2000).
[6] R. Van Roij, M. Dijstra and R. Evans, Europhys. Lett. **49**, 350 (2000); J. Chem. Phys. **113**, 7689 (2000).
[7] Y. Martínez-Ratón, cond-mat/0212333 (2002).
[8] J. A. C. Veerman and D. Frenkel, Phys. Rev. A **45**, 5632 (1992).
[9] P. Bolhuis and D. Frenkel, J. Chem. Phys. **106**, 666 (1997).
[10] A. Casey and P. Harrowell, J. Chem. Phys. **103**, 6143 (1995).
[11] R. van Roij and B. Mulder, J. Phys. II (France) **4**, 1763 (1994).
[12] R. Alben, J. Chem. Phys. **59**, 4299 (1973).
[13] J. A. Cuesta and Y. Martínez-Ratón, Phys. Rev. Lett. **78**, 3681 (1997).
[14] Y. Martínez-Ratón and J. A. Cuesta, Phys. Rev. Lett.

89, 185701 (2002).
[15] F. M. van der Kooij and H. N. W. Lekkerkerker, Phys. Rev. Lett. **84**, 781 (2000).
[16] H. H. Wensink, G. J. Vroege and H. N. W. Lekkerkerker, J. Chem. Phys. **115**, 7319 (2001).
[17] A. M. Bohle, R. Holyst and T. Vilgis, Phys. Rev. Lett. **76**, 1396 (1996).
[18] M. A. Bates and D. Frenkel, Phys. Rev. E **57**, 4824 (1998).
[19] Y. Rosenfeld, Phys. Rev. Lett. **63**, 980 (1989).
[20] J. A. Cuesta, Europhys. Lett. **46**, 197 (1999).
[21] P. Sollich, J. Phys.: Condens. Matt. **14**, R79 (2002).
[22] Y. Martínez-Ratón and J. A. Cuesta, J. Chem. Phys. **111**, 317 (1999).
[23] J. M. Polson and D. Frenkel, Phys. Rev. E **56**, R6260 (1997).
[24] L. Lafuente and J. A. Cuesta, Phys. Rev. Lett. **89**, 145701 (2002).
[25] P. J. Camp, M. P. Allen, P. G. Bolhuis and D. Frenkel, J. Chem. Phys. **106**, 9270 (1997).
[26] H. H. Wensink, G. J. Vroege and H. N. W. Lekkerkerker, Phys. Rev. E **66**, 041704 (2002).
[27] A. Stroobants, J. Phys.: Condens. Matt. **6**, A285 (1994).